materials

MDPI

Article

Superionic Solid Electrolyte $Li_7La_3Zr_2O_{12}$ Synthesis and Thermodynamics for Application in All-Solid-State Lithium-Ion Batteries

Daniil Aleksandrov [1,*], Pavel Novikov [1], Anatoliy Popovich [1] and Qingsheng Wang [2]

[1] Institute of Machinery, Materials, and Transport, Peter the Great St. Petersburg Polytechnic University, 195251 Saint Petersburg, Russia; novikov_pa@spbstu.ru (P.N.); director@immet.spbstu.ru (A.P.)

[2] CHN/RUS New Energy and Material Technology Research Institute, Huzhou 313100, China; envbattery@yandex.ru

* Correspondence: aleksandrov_ds@spbstu.ru

Abstract: Solid-state reaction was used for $Li_7La_3Zr_2O_{12}$ material synthesis from Li_2CO_3, La_2O_3 and ZrO_2 powders. Phase investigation of $Li_7La_3Zr_2O_{12}$ was carried out by x-ray diffraction (XRD), scanning electron microscopy (SEM) and energy-dispersive x-ray spectroscopy (EDS) methods. The thermodynamic characteristics were investigated by calorimetry measurements. The molar heat capacity ($C_{p,m}$), the standard enthalpy of formation from binary compounds ($\Delta_{ox}H_{LLZO}$) and from elements ($\Delta_f H_{LLZO}$), entropy ($S^0{}_{298}$), the Gibbs free energy of the $Li_7La_3Zr_2O_{12}$ formation ($\Delta_f\ G^0{}_{298}$) and the Gibbs free energy of the LLZO reaction with metallic Li ($\Delta_r G_{LLZO/Li}$) were determined. The corresponding values are $C_{p,m}$ = 518.135 + 0.599 × T − 8.339 × T^{-2}, (temperature range is 298–800 K), $\Delta_{ox}H_{LLZO}$ = −186.4 kJ·mol^{-1}, $\Delta_f H_{LLZO}$ = −9327.65 ± 7.9 kJ·mol^{-1}, $S^0{}_{298}$ = 362.3 J·mol^{-1}·K^{-1}, $\Delta_f\ G^0{}_{298}$ = −9435.6 kJ·mol^{-1}, and $\Delta_r G_{LLZO/Li}$ = 8.2 kJ·mol^{-1}, respectively. Thermodynamic performance shows the possibility of $Li_7La_3Zr_2O_{12}$ usage in lithium-ion batteries.

Keywords: lithium-ion battery; solid-state electrolyte; lithium-ion thermodynamics; solid-state synthesis

check for updates

Citation: Aleksandrov, D.; Novikov, P.; Popovich, A.; Wang, Q. Superionic Solid Electrolyte $Li_7La_3Zr_2O_{12}$ Synthesis and Thermodynamics for Application in All-Solid-State Lithium-Ion Batteries. *Materials* **2022**, *15*, 281. https://doi.org/10.3390/ma15010281

Academic Editor: Alessandro DellEra

Received: 9 December 2021
Accepted: 27 December 2021
Published: 31 December 2021

1. Introduction

The commercial history of the lithium-ion battery was started in 1991 by Sony [1]. Since then, a lot of effort has been directed to improving the electrochemical performance of lithium-ion batteries [2]. One of the perspective methods of stabilizing lithium-ion battery electrochemical characteristics and safety is to apply solid-state inorganic electrolyte instead of liquid organic electrolyte as the traditional electrolyte for commercial lithium-ion batteries [3–7]. Some solid-state electrolytes have high ionic conductivity in an order of magnitude of ~10^{-3} S·cm^{-1} [8] in comparison to liquid electrolyte [9].

Between all types of the solid-state electrolytes (perovskite, NASICON- and LISICON-type, LATP- and LAGP-type, garnet, sulfide and halide electrolytes, etc. [8]) garnet-type electrolytes have the most attractive electrochemical performance in combination with manufacturing costs and simplicity in commercial application. Garnet-type $Li_7La_3Zr_2O_{12}$ (LLZO) solid-state electrolyte has two modifications: cubic and tetragonal. The ionic conductivities are ~10^{-4}–10^{-3} S·cm^{-1} and ~10^{-7}–10^{-6} S·cm^{-1}, respectively [10].

LLZO solid-state electrolyte attracts high attention due to its relatively high electrochemical properties. Though LLZO has lower ionic conductivity in comparison with organic liquid electrolyte (~10^{-4} versus ~10^{-2} S·cm^{-1}, respectively [9]), it provides high safety performance, high chemical stability against metallic lithium, a wide electrochemical potential window, low electronic conductivity, and high stability with moisture in the air; LLZO prevents lithium dendrite growth due to high mechanical strength [11–15].

Since as LLZO was first synthesized by Murugan et al. [16], it was investigated to improve its chemical and structural stability, long life cycle, electrode/solid electrolyte

interface interactions, and high energy density at room temperature. Thus, heterovalent substitution/doping with Al^{3+} from alumina crucible (or intentional incorporation) during the synthesis process allows for the enhancement of ionic conductivity up to ~10^{-3} S·cm^{-1}, but it causes higher activation energy in lithium ion conduction, which limits Li^{+} mobility [17–24]. Doped with Ga^{3+} also as Al^{3+} stabilize structure of LLZO [25–32]. The substitution of Zr^{4+} with Ta^{5+} ions allowed for an increase of the ionic conductivity, stabilization of the cubic structure, improved lithium-ion transport, lithium dendrite growth prevention, and the current density [33–38]. Ultimately, the above-mentioned elements improve electrochemical and structural stability, increase the ionic conductivity, and prevent lithium dendrite growth and penetration at the solid electrolyte structure.

In this work, synthesis, structure studies and thermodynamics calculations of tetragonal $Li_7La_3Zr_2O_{12}$ were performed.

2. Materials and Methods

Tetragonal LLZO electrolyte was produced by solid-state synthesis as one of the commonly used synthesis methods for investigation and mass manufacture [39–47]. Initial materials Li_2CO_3 (Xilong Sci., 99%), La_2O_3 (ReLAB, 99.99%), and ZrO_2 (Sinopharm, 99.9%) in stoichiometric ratio were used as sources for Li, La, and Zr, respectively. Excess of 10 wt.% of lithium was initially added to precursor to avoid lithium loss during the synthesis process at high temperatures. Lanthanum oxide was preliminarily dried at 900 °C for 24 h. The mentioned materials were mechanically milled in an agate mortar and then dissolved in acetic acid with subsequent magnetic stirring at 90 °C for 12 h to provide a homogeneous solution. Excess acetic acid was evaporated at 110 °C to get dry precursor powder. Dried precursor was then mechanically milled in an agate mortar and put into an alumina crucible for heat treatment. A muffle furnace (Nabertherm, Lilienthal, Germany) was used for solid-state reaction at air atmosphere. First, the precursor was slowly heated (heat rate was 0.5 °C/min) to 130 °C for 3 h to evaporate the remaining acetic acid. Then, the precursor was heated (heat rate was 2 °C/min) to 900 °C for 8 h to provide solid-state reaction.

The solid-state reaction proceeds according to next formula:

$$4ZrO_2 + 3La_2O_3 + 7Li_2CO_3 = 2Li_7La_3Zr_2O_{12} + 7CO_2 \quad (1)$$

X-ray diffraction structural analysis (XRD) was performed by Bruker D8 Advance (Bruker, Karlsruhe, Germany) equipment (diffraction angle step was 0.02°, Cu K_α-radiation). The Rietveld method was used for structure refinement. Diffraction angles for synthesized LLZO powder were set from 15° to 60° (2Θ).

Images of the microstructure performance of LLZO powder were taken with a scanning electron microscope (SEM) Tescan MAIA3 (Tescan, Brno, Czech Republic) with secondary electron detection. Bruker XFlash 6–10 (Bruker, Karlsruhe, Germany) was used for energy-dispersive X-ray spectroscopy (EDS).

TAM IV Microcalorimeter (TA Instruments, Shanghai, China) was used for calorimetric investigation. Measurement parameters were as follows: temperature is 298 K, volume of the cell is 20 mL. An aqueous solution of 1 mol·dm^{-3} HCl was filled in the ampoule at calorimetric cell. The dissolution process of the LLZO powder was started after thermal equilibrium was established. Dissolution enthalpy value was obtained from thermoelectromotive force data during the dissolution process, providing the heat dissolution curve.

3. Results

The XRD pattern of synthesized LLZO is shown at Figure 1. According to diffraction data, LLZO has a $I4_1/acd$ space group. The vertical lines at the bottom are related to PDF #00-064-0140. The peak indexes and interplanar distances are shown in the Supplementary Materials (Table S1). Synthesized material contains 4 wt.% of La_2O_3 impurity after solid-state reaction.

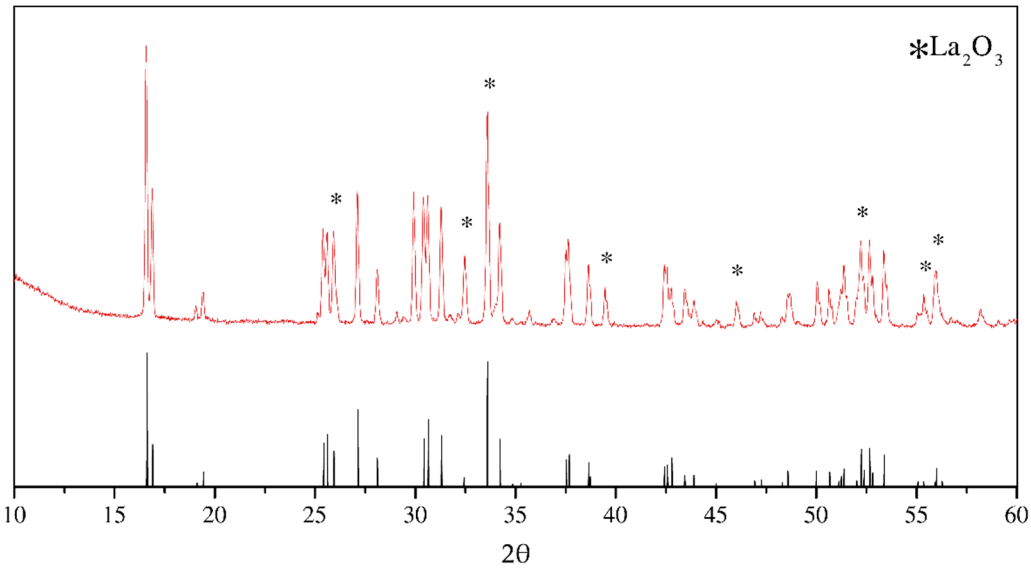

Figure 1. X-ray diffraction pattern of the synthesized tetragonal $Li_7La_3Zr_2O_{12}$ by solid-state reaction. Bottom vertical lines belong to PDF #00-064-0140.

SEM images of LLZO powder are shown in Figure 2, made at 2×, 3.5×, 10× and 11.5× magnification, respectively. All images were performed at 10 keV landing energy.

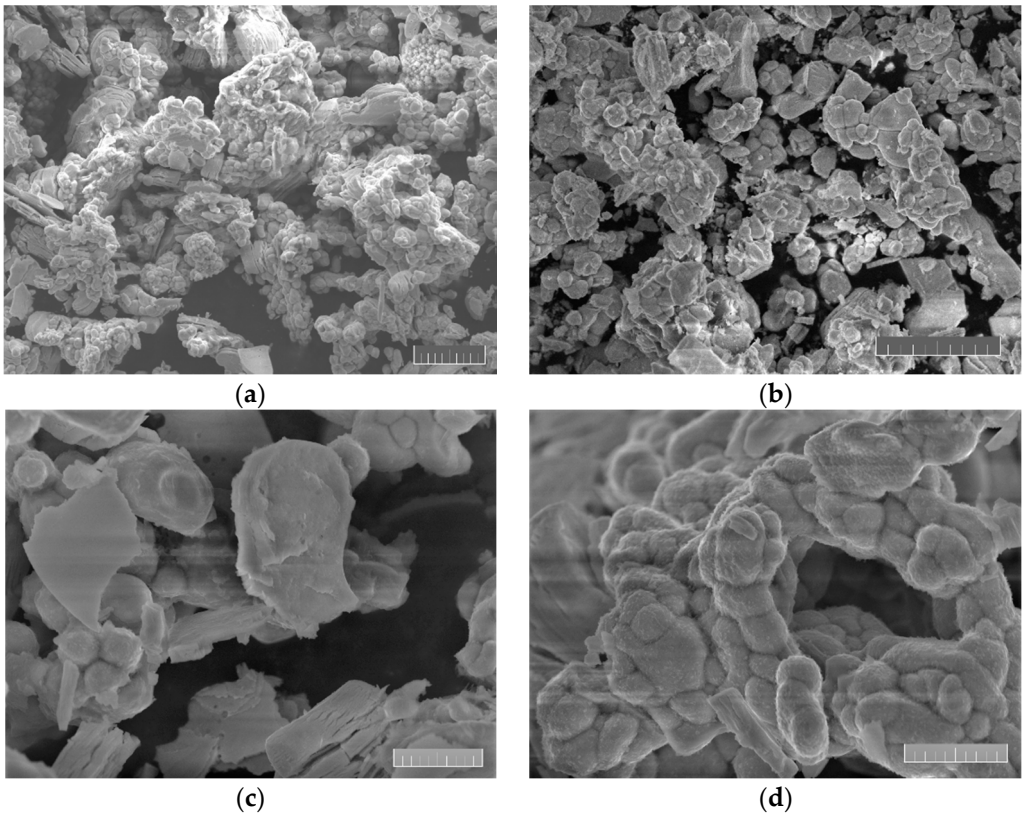

Figure 2. SEM images of synthesized LLZO powder at different magnification. The scale bar is (**a**,**b**) 20 µm and (**c**,**d**) 5 µm long.

EDS spectra images are shown at Figure 3. The scale bar is 80 µm long for all images at Figure 3a–d. The green frame in Figure 3a shows the EDS analyzing field. Figure 3b–d show the element distributions for the La, Zr, O and C at Figure 3b; La at Figure 3c; and Zr at Figure 3d elements, respectively. The elements in Figure 3 are evenly distributed. The

carbon in Figure 3b is electrically conductive carbon tape for sample holder. Elemental analysis of EDS spectra is shown at Table 1.

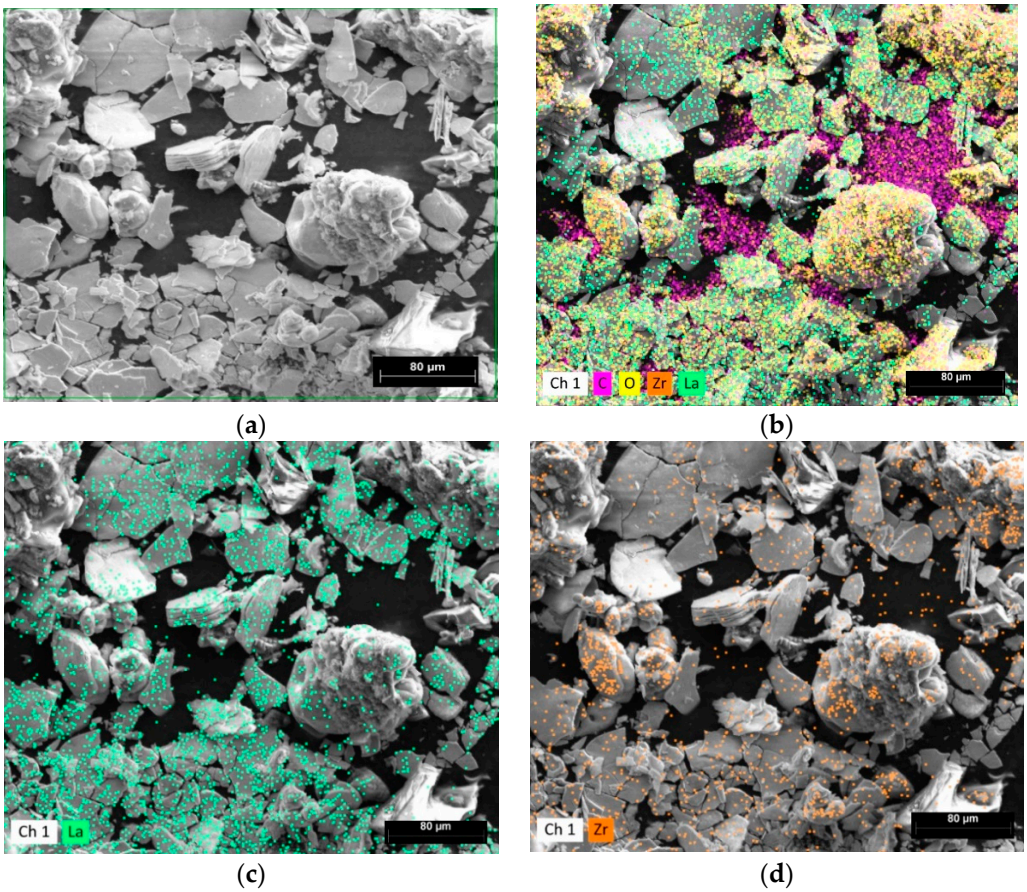

Figure 3. SEM images of the synthesized LLZO powder at different magnifications. The scale bar is (**a**,**b**) 20 µm, and (**c**,**d**) 5 µm long.

Table 1. Elemental EDS analysis of $Li_7La_3Zr_2O_{12}$ powder.

Element	Mass, wt.%
Lanthanum	53.19
Oxygen	22.59
Zirconium	24.22

EDS elemental analysis of the LLZO powder shows lanthanum excess in the solid electrolyte powder, expressed in terms of $Li_7La_3Zr_2O_{12}$ and La_2O_3 compounds. Elemental analysis based on Table 1 shows an excess of 3.1 wt.% of lanthanum oxide (III).

4. Discussion

4.1. The Standard Formation Enthalpy

The formation enthalpy of $Li_7La_3Zr_2O_{12}$ ($\Delta_{ox}H_{LLZO}$) from Li_2CO_3, La_2O_3, and ZrO_2 is calculated according to Equation (1) from the Experimental Section. The subscript *ox* means "oxides", which relates to the initial compounds from Equation (1).

The following thermodynamic cycle was used for enthalpy calculation, Figure 4:

$$Li_7La_3Zr_2O_{12} + 24HCl_{(aq)} \rightarrow 7LiCl_{(aq)} + 3LaCl_{3(aq)} + 2ZrCl_{4(aq)} + 12H_2\uparrow + 6O_2\uparrow, \quad (2)$$

$$Li_2CO_3 + 2HCl_{(aq)} \rightarrow 2LiCl + CO_2 + H_2O, \quad (3)$$

$$La_2O_3 + 6HCl_{(aq)} \rightarrow 2LaCl_3 + 3H_2O, \quad (4)$$

$$ZrO_2 + 4HCl_{(aq)} \rightarrow ZrCl_4 + 2H_2O, \quad (5)$$

the subscript *(aq)* indicates "aqueous". The calorimeter was used for the standard enthalpy ($\Delta_d H_{LLZO}$) measurement. The received value after calorimetry measurement was equal to -1911 ± 37 J·g^{-1}, Table 2.

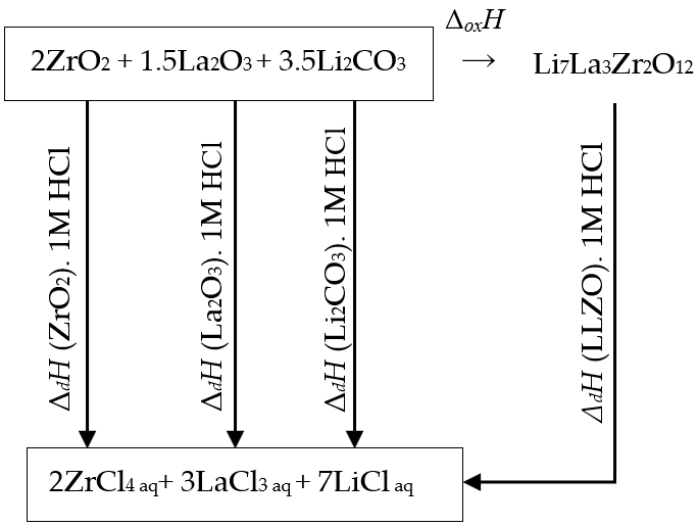

Figure 4. Diagram of the thermochemical dissolution cycle of $Li_7La_3Zr_2O_{12}$ in HCl.

Table 2. The dissolution enthalpies values of the initial components and the $Li_7La_3Zr_2O_{12}$ compound (p = 101 kPa, T = 298 K, 1 mol·dm^{-3} $HCl_{(aq)}$).

Compound	Molar Mass, g·mol^{-1}	Specific Enthalpy, J·g^{-1}	Molar Enthalpy of Dissolution, kJ·mol^{-1}	Ref.
ZrO_2	123.222	-2186 ± 19	-269.4 ± 2.34	this work
La_2O_3	325.837	-1927 ± 13	-627.9 ± 4.23	this work
Li_2CO_3	73.89	-683 ± 9	-50.5 ± 0.67	this work
$Li_7La_3Zr_2O_{12}$ (with La_2O_3 impurity)	-	-1758 ± 34	-	this work
$Li_7La_3Zr_2O_{12}$	839.741	-1752.6 ± 35	-1471.73 ± 29.39	this work (recalculated)

It was shown in the Experimental Section that LLZO has 3.1 wt.% of unreacted La_2O_3 impurity. Thereby, measured $\Delta_d H_{LLZO}$ should be recalculated considering the amount of La_2O_3:

$$\Delta_d H_{LLZO} = \frac{\Delta_d H_{LLZO+La_2O_3} - \omega \Delta_d H_{La_2O_3}}{1 - \omega}, \quad (6)$$

where ω is the mass fraction of La_2O_3. It should be noted that enthalpies, mentioned in Equation (6), are supposed to be specific, not molar. The recalculated value of the dissolution enthalpy of LLZO (with 3.1 wt.% of La_2O_3) is equal to -1917.7 J·g^{-1} or -1607.75 kJ·mol^{-1}, Table 2.

The formation enthalpy value of $\Delta_{ox} H_{LLZO}$ is estimated by the next formula:

$$\Delta_{ox} H_{LLZO} = 2\Delta_d H_{ZrO_2} + 1.5\Delta_d H_{La_2O_3} + 3.5\Delta_d H_{Li_2CO_3} - \Delta_d H_{LLZO} \quad (7)$$

The calorimetry-measured values of $\Delta_d H_{ZrO_2}$, $\Delta_d H_{La_2O_3}$, and $\Delta_d H_{Li_2CO_3}$ are shown in Table 2. The recalculated value of the enthalpy of dissolution of $Li_7La_3Zr_2O_{12}$ was

used for $\Delta_{ox}H_{LLZO}$ evaluation. The value of $\Delta_{ox}H_{LLZO}$ given by Equation (7) is equal to -186.4 kJ mol^{-1}. The negative value of the enthalpy of $Li_7La_3Zr_2O_{12}$ formation indicates that $Li_7La_3Zr_2O_{12}$ is a stable phase; the chemical reaction of Li_2CO_3, La_2O_3, and ZrO_2 is energetically favorable for $Li_7La_3Zr_2O_{12}$ synthesis. The values for various lithium zirconates were added to Table 2 to compare with the measured and calculated values in this work. The value of the formation enthalpy from binary oxides $\Delta_{ox}H_{LLZO}$ has the same order as corresponding values for lithium zirconate compounds and complex oxides (Table 3), thus it can be concluded that the measurements are correct.

Table 3. Standard enthalpies of formation of complex oxides from binary oxides ($\Delta_{ox}H^0$).

Compound	$\Delta_{ox}H^\circ_{298.15}$, kJ·mol^{-1}	Reference
$Li_7La_3Zr_2O_{12}$ (s)	-186.4 ± 7.3	this work
Li_2ZrO_3 (s)	-304.1 ± 1.4	[48]
$Li_6Zr_2O_7$ (s)	-112.86	[49]
$La_2Zr_2O_7$ (s)	-135.6	[50]
Li_2TiO_3 (s)	-238.5 ± 1.5	[48]
$LiAlO_2$ (s)	-209.0 ± 3.2	[4]
$LiCoO_2$ (s)	-143.99 ± 1.38	[51]
$BaZrO_3$ (s)	-114.6	[52]

The subscripts (s) mean "solid".

Finally, the enthalpy of $Li_7La_3Zr_2O_{12}$ formation from elements can be calculated by the following formula:

$$\Delta_f H_{LLZO} = 3.5\Delta_f H_{Li_2CO_3} + 1.5\Delta_f H_{La_2O_3} + 2\Delta_f H_{ZrO_2} + \Delta_{ox}H_{LLZO} \quad (8)$$

The corresponding handbook's materials were used to define the standard enthalpies [53], Table 4.

Table 4. Standard enthalpies of formation from elements ($\Delta_f H^0$).

Material	$\Delta_f H^\circ_{298.15}$, kJ·mol^{-1}	Ref.
Li_2CO_3 (s)	-1214.1 ± 1.0	[53]
La_2O_3 (s)	-1794.2 ± 2.0	[53]
ZrO_2 (s)	-1100.3 ± 0.7	[53]
$Li_7La_3Zr_2O_{12}$ (s)	-9327.65 ± 7.9	this work

The subscripts (s) mean "solid".

The formation enthalpy value of the $Li_7La_3Zr_2O_{12}$ compound, calculated by formula (8) is -9327.65 ± 7.9 kJ·mol^{-1}, Table 4. The enthalpy of formation value, rated by Equation (8), can be recommended for use in further thermodynamic calculations of $Li_7La_3Zr_2O_{12}$ reactivity.

4.2. The Isobaric Heat Capacity

Figure 5 shows the isobaric heat capacity of the $Li_7La_3Zr_2O_{12}$ as a function of temperature ($C_p = f(T)$). Pay attention to the certain amount of La_2O_3 (Figure 1 and Table 1) in LLZO synthesized powder material, the measured isobaric heat capacity for the two-phase system must be recalculated by the following additive rule:

$$mC_p = m(LLZO)C_p(LLZO) + m(La_2O_3)C_p(La_2O_3), \quad (9)$$

where C_p is a specific heat capacity (p = const), and m is mass. In our case, the two-phase system consists of the solid electrolyte compound (LLZO) and La_2O_3. Thus, the heat capacity of $Li_7La_3Zr_2O_{12}$ is expressed from Equation (9) as:

$$C_p(LLZO) = \frac{mC_p - m(La_2O_3)C_p(La_2O_3)}{m(LLZO)} \tag{10}$$

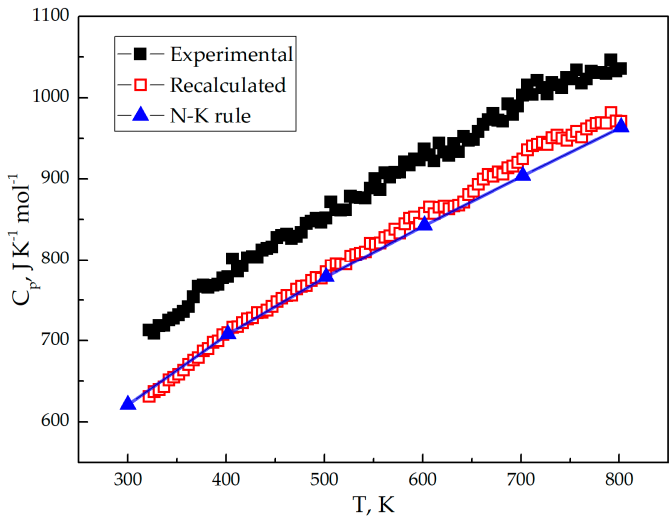

Figure 5. The experimental (filled square), recalculated (unfilled square) and Neumann-Kopp rule (line-connected triangles) heat capacities of $Li_7La_3Zr_2O_{12}$.

The impurity compound weight can be recalculated from the total weight of the sample, with the known mass fraction of lanthanum oxide, $\omega(La_2O_3)$:

$$m(La_2O_3) = m\omega(La_2O_3) \tag{11}$$

and

$$m(LLZO) = m[1 - \omega(La_2O_3)] \tag{12}$$

Considering Equations (11) and (12), Equation (13) can be expressed as follows:

$$C_p(LLZO) = \frac{C_p - C_p(La_2O_3)\omega(La_2O_3)}{1 - \omega(La_2O_3)} \tag{13}$$

Equation (13) shows, that the $Li_7La_3Zr_2O_{12}$ heat capacity $C_p(LLZO)$ can be evaluated by the measured heat capacity (C_p), tabulated heat capacity of La_2O_3 $C_p(La_2O_3)$, and La_2O_3 mass fraction $\omega(La_2O_3)$. The dependence of La_2O_3 specific heat capacity from temperature is required for Equation (13) calculation. For this, tabular data is required to define temperature dependence for the lanthanum oxide heat capacity [53]. The heat capacity polynomial, commonly used for the low temperature range (for 300–800 K in our case) can be expressed as follows:

$$C_p = a + bT - cT^{-2} \tag{14}$$

where a, b, and c are empirical coefficients, and T is the absolute temperature. The La_2O_3 received coefficients are a = 119.604 J·mol^{-1}·K^{-1}, b = 14.514 × 10^{-3} J·mol^{-1}·K^{-2}, and c = 13.452 × 10^5 J·mol^{-1}·K. Considering the La_2O_3 impurity presence, the LLZO heat capacity can be recalculated via Equations (13) and (14) for the 300–800 K temperature interval. According to XRD and EDS data (Figure 1 and Table 1, respectively) LLZO contains about 3.1 ± 0.12 wt.% La_2O_3. Figure 5 and Table 5 shows measured and recalculated LLZO heat capacity temperature dependence. The Neumann-Kopp (N-K) rule was used for the empirical value calculation of the heat capacity. The N-K rule approves "that the molecular

heat capacity of a solid compound is the sum of the atomic heat capacities of the elements composing it; the elements having atomic heat capacities lower than those required by the Dulong–Petit law retain these lower values in their compounds." [54]. This rule commonly gives reproducible results for room temperatures, not for high temperatures. To achieve more accurate results, binary materials were used instead of single elements (accurate results are usually obtained for the same aggregate state of materials):

$$C_p(CO) = \sum n(BO)C_p(BO) \tag{15}$$

C_p is a molar heat capacity (p = const), n is a stoichiometric coefficient, and CO and BO are complex and binary oxide, respectively. Equation (15), considering Equation (1), can be expressed for LLZO as follows:

$$C_p(LLZO) = 3.5C_p(Li_2CO_3) + 1.5C_p(La_2O_3) + 2C_p(ZrO_2) \tag{16}$$

The calculated from tabular data [53] heat capacity from Equation (16) is shown on Figure 5 and Table 5.

Table 5. The $Li_7La_3Zr_2O_{12}$ (s) heat capacities of experimental C_p(exp.), recalculated by Equation (15) C_p(rec.) and calculated by the (N-K) rule C_p(N-K) values as a function of temperature.

T, K	C_p(exp.), J·K^{-1}·mol^{-1}	C_p(rec.), J·K^{-1}·mol^{-1}	C_p(N-K), J·K^{-1}·mol^{-1}
300	-	-	621.1
400	778.6	709.7	708.1
500	851.8	784.7	778.8
600	936.7	857.4	843.1
700	1002.8	925.0	904.3
800	1035.4	971.1	964.0

The Neumann-Kopp rule and recalculated heat capacity of $Li_7La_3Zr_2O_{12}$ are in good correlation. Experimental data is for the LLZO compound with La_2O_3 impurity. The heat capacity temperature dependence (Equation (16)) was calculated using tabular data [53,55]. XRD and EDS quantitative analysis gives accurate enough results to define a small quantity of impurity compounds in the material.

4.3. Entropy

The Third Law of Thermodynamics states, "The entropy of a perfect crystal is zero when the temperature of the crystal is equal to absolute zero (0 K)." Thus, the entropy absolute value can be valued by the equation:

$$S(T) = \int_0^{T_1} \frac{C_p(T)}{T} dT + \frac{\Delta H_1}{T_1} + \int_{T_1}^{T_2} \frac{C_p(T)}{T} dT + \frac{\Delta H_2}{T_2} + \ldots + \int_{T_k}^{T} \frac{C_p(T)}{T} dT, \tag{17}$$

where S is entropy, T_k is temperature of the k-th phase transition ($0 < T_k < T$), and ΔH_k is enthalpy of the k-th phase transition. The Neumann-Kopp rule for entropy calculation can be expressed as follows (considering absence of phase transition at calculating temperature range):

$$S(T) = \int_0^{T} \frac{\sum C_p(T,\ BO)}{T} dT = \sum \int_0^{T} \frac{C_p(T,\ BO)}{T} dT = \sum S(T, BO), \tag{18}$$

where *BO* is the binary oxide compound (see Equation (15)). Equation (18) can be rewritten taking into account Equations (15) and (16):

$$S\ (LLZO) = 3.5S(Li_2CO_3) + 1.5S(La_2O_3) + 2S(ZrO_2) \quad (19)$$

The $Li_7La_3Zr_2O_{12}$ entropy is equal to 607.18 J·mol^{-1}·K^{-1} (T = 298 K) by calculating Equation (19) using tabulated data [53,55]. The additive rule for entropy calculation can be used if the following term is met: the complex compound molar volume slightly differs of the molar volumes sum of binary compounds [55]. Thus, the molar volume for Li_2CO_3 is 35.0 cm^3·mol^{-1} (density is ρ = 2.11 g·cm^{-3} [56]), for La_2O_3 is 50.1 cm^3·mol^{-1} (density is ρ = 6.51 g·cm^{-3} [57]), for ZrO_2 is 21.2 cm^3·mol^{-1} (density is ρ = 5.56 g·cm^{-3} [57]), and for $Li_7La_3Zr_2O_{12}$ is 165.0 cm^3·mol^{-1} (density is ρ = 5.09 g·cm^{-3} [58]). The sum of the molar volumes of Li_2CO_3, La_2O_3, and ZrO_2 with their corresponding stoichiometric coefficients is 240.05 cm^3·mol^{-1} and differs about 45.5% of the LLZO molar volume, which does not allow one to apply the additive rule.

Excepting the additive calculation rule, the W. Herz rule can be used for the LLZO entropy calculation [59]:

$$S^0_{298} = K_H\left(M/C_{p,298}\right)^{1/3}m, \quad (20)$$

where K_H is the Herz constant, M is molar mass, $C_{p,298}$ is isobaric heat capacity, and m is atoms per formula.

The Herz constant K_H has a good correlation with average values of anion molar mass [60]:

$$K_H = \frac{33.5x^2e^x}{\left(e^x - 1\right)^2}, \quad (21)$$

where $x = 42.4/M_{La_3Zr_2O_{12}}$, and M_A is an anion ($La_3Zr_2O_{12}{}^{7-}$) molar mass. For $Li_7La_3Zr_2O_{12}$, anion molar mass $M_{La_3Zr_2O_{12}}$ is 791.154 g·mol^{-1}. Thus, K_H constant is equal to 33.5.

Considering $C_{p,298}$ from Table 5 and Equation (21), calculated by Equation (20) the LLZO entropy is equal to 362.3 J mol^{-1}·K^{-1}. The calculated value of LLZO entropy by the W. Herz rule is in good correlation with Ref. [60]. Hence, the N-K rule cannot be used for the entropy calculations, as follows from molar masses principle.

4.4. The Standard Gibbs Free Energy

Calculated formation enthalpy and entropy allows one to rate the standard Gibbs free energy ($\Delta_f G^0_{298}$) of LLZO formation (T = 298 K):

$$\Delta_f G^0_{298} = \Delta_f H^0_{298} - 298\Delta_f S^0_{298}, \quad (22)$$

For Equation (22), the $\Delta_f G^0_{298}$ value of LLZO is equal to −9435.6 kJ·mol^{-1}.

The stability against metallic lithium can be estimated by the Gibbs free energy calculation of the following reaction at room temperature:

$$3Li + Li_7La_3Zr_2O_{12} = 7.5Li_2O + 1.5La_2O_3 + 2Zr \quad (23)$$

The Gibbs free energy of reaction ($\Delta_r G_{LLZO/Li}$) can be expressed as the difference between the and the Gibbs energy values of reactants and resultants of the reaction. The $\Delta_f G^0_{298}$ for single elements is equal to zero, for Li_2O is −561.2 kJ·mol^{-1}, and for La_2O_3 is −1706.7 kJ·mol^{-1} [53]. The $Li_7La_3Zr_2O_{12}$ Gibbs free energy has been calculated above. Thus, the Gibbs free energy for reaction (23) is $\Delta_r G_{LLZO/Li}$ = 8.2 kJ·mol^{-1}; this means that the reaction is thermodynamically impossible. Finally, $Li_7La_3Zr_2O_{12}$ is stable against metallic lithium at room temperature.

5. Conclusions

The thermodynamic characteristics were determined for $Li_7La_3Zr_2O_{12}$ solid-state electrolyte material for lithium-ion battery. Solid-state reaction was used as the synthesis

method of $Li_7La_3Zr_2O_{12}$ from Li_2CO_3, La_2O_3, and ZrO_2. The synthesized material had 3.1 wt.% of the lanthanum oxide (La_2O_3) impurity according to XRD and EDS data. Probably, this amount of La_2O_3 is unreacted oxide from the synthesis process. The enthalpy of $Li_7La_3Zr_2O_{12}$ formation from binary oxides (and from Li_2CO_3) $\Delta_{ox}H_{LLZO}$ and from the elements $\Delta_f H_{LLZO}$ were calculated according to the measured enthalpy of dissolution of reagents and the products of the $Li_7La_3Zr_2O_{12}$ formation reaction. The obtained values are equal to -186.4 ± 7.3 kJ·mol^{-1} and -9327.65 ± 7.9, respectively. The formation enthalpy from binary oxides $\Delta_{ox}H_{LLZO}$ is in good correlation with similar zirconate compounds, which confirms the correctness of the measurements.

The recalculated LLZO heat capacity considering La_2O_3 presence is in good correlation with that calculated by the Neumann-Kopp rule. Finally, the temperature dependence of the LLZO heat capacity can be expressed by the formula $C_p(T) = 518.135 + 0.599 \times T - 8.339 \times T^{-2}$ (T is absolute temperature). The LLZO entropy is $S^0_{298} = 362.3$ J·mol^{-1}·K^{-1}, the Gibbs free energy of formation of $Li_7La_3Zr_2O_{12}$ is -9435.6 kJ mol^{-1}. $Li_7La_3Zr_2O_{12}$ material is stable against metallic lithium, according to the Gibbs free energy of the LLZO reaction with metallic Li. All thermodynamic values and functions measured and calculated for $Li_7La_3Zr_2O_{12}$ can be used for modelling and further calculations of all-solid-state batteries.

Supplementary Materials: The following supporting information can be downloaded at: https://www.mdpi.com/article/10.3390/ma15010281/s1, Table S1: HKL indexes for XRD pattern (corresponding to Figure 1).

Author Contributions: Conceptualization, A.P. and P.N.; methodology, D.A.; software, D.A.; validation, D.A. and Q.W.; formal analysis, A.P.; investigation, D.A.; resources, Q.W.; data curation, P.N.; writing—original draft preparation, D.A.; writing—review and editing, P.N.; visualization, D.A.; supervision, A.P.; project administration, Q.W.; funding acquisition, Q.W. All authors have read and agreed to the published version of the manuscript.

Funding: The research is partially funded by the Ministry of Science and Higher Education of the Russian Federation: Advanced Digital Technologies (contract No. 075-15-2020-934 dated from 17.11.2020).

Institutional Review Board Statement: Not applicable.

Informed Consent Statement: Not applicable.

Data Availability Statement: The data presented in this study are available on request from the corresponding author.

Conflicts of Interest: The authors declare no conflict of interest.

References

1. Nishi, Y. Lithium-ion secondary batteries; past 10 years and the future. *J. Power Sources* **2001**, *100*, 101–106. [CrossRef]
2. Ma, J.; Li, Y.; Grundish, N.S.; Goodenough, J.B.; Chen, Y.; Guo, L.; Peng, Z.; Qi, X.; Yang, F.; Qie, L.; et al. The 2021 battery technology roadmap. *J. Phys. D Appl. Phys.* **2021**, *54*, 183001. [CrossRef]
3. Horowitz, Y.; Schmidt, C.; Yoon, D.H.; Riegger, L.M.; Katzenmeier, L.; Bosch, G.M.; Noked, M.; Ein-Eli, Y.; Janek, J.; Zeier, W.G.; et al. Between Liquid and All Solid: A Prospect on Electrolyte Future in Lithium-Ion Batteries for Electric Vehicles. *Energy Technol.* **2020**, *8*, 2000580. [CrossRef]
4. Han, L.; Lehmann, M.L.; Zhu, J.; Liu, T.; Zhou, Z.; Tang, X.; Heish, C.T.; Sokolov, A.P.; Cao, P.; Chen, X.C.; et al. Recent Developments and Challenges in Hybrid Solid Electrolytes for Lithium-Ion Batteries. *Front. Energy Res.* **2020**, *8*, 202. [CrossRef]
5. Tan, D.H.; Chen, Y.T.; Yang, H.; Bao, W.; Sreenarayanan, B.; Doux, J.M.; Li, W.; Lu, B.; Ham, S.Y.; Sayahpour, B.; et al. Carbon-free high-loading silicon anodes enabled by sulfide solid electrolytes. *Science* **2021**, *373*, 1494–1499. [CrossRef] [PubMed]
6. Byeon, Y.W.; Kim, H. Review on Interface and Interphase Issues in Sulfide Solid-State Electrolytes for All-Solid-State Li-Metal Batteries. *Electrochem* **2021**, *2*, 30. [CrossRef]
7. Tripathi, A.K. Ionic liquid based solid electrolytes (ionogels) for application in rechargeable lithium battery. *Mater. Today Energy* **2021**, *20*, 100643. [CrossRef]
8. Yu, T.; Yang, X.; Yang, R.; Bai, X.; Xu, G.; Zhao, S.; Duan, Y.; Wu, Y.; Wang, J. Progress and perspectives on typical inorganic solid-state electrolytes. *J. Alloys Compd.* **2021**, *885*, 161013. [CrossRef]
9. Chan, C.K.; Yang, T.; Weller, J.M. Nanostructured garnet-type $Li_7La_3Zr_2O_{12}$: Synthesis, properties, and opportunities as electrolytes for Li-ion batteries. *Electrochim. Acta* **2017**, *253*, 268–280. [CrossRef]

10. Shen, Z.; Zhang, W.; Zhu, G.; Huang, Y.; Feng, Q.; Lu, Y. Design Principles of the Anode–Electrolyte Interface for All Solid-State Lithium Metal Batteries. *Small Methods* **2020**, *4*, 1900592. [CrossRef]
11. Tikekar, M.D.; Choudhury, S.; Tu, Z.; Archer, L.A. Design principles for electrolytes and interfaces for stable lithium-metal batteries. *Nat. Energy* **2016**, *1*, 16114. [CrossRef]
12. Wang, H.; Yu, D.; Kuang, C.; Cheng, L.; Li, W.; Feng, X.; Zhang, Z.; Zhang, X.; Zhang, Y. Alkali metal anodes for rechargeable batteries. *Chem* **2019**, *5*, 313–338. [CrossRef]
13. Famprikis, T.; Canepa, P.; Dawson, J.A.; Islam, M.S.; Masquelier, C. Fundamentals of inorganic solid-state electrolytes for batteries. *Nat. Mater.* **2019**, *18*, 1278–1291. [CrossRef] [PubMed]
14. Zhang, Z.; Shao, Y.; Lotsch, B.; Hu, Y.S.; Li, H.; Janek, J.; Nazar, L.F.; Nan, C.W.; Maier, J.; Armand, M.; et al. New horizons for inorganic solid state ion conductors. *Energy Environ. Sci.* **2018**, *11*, 1945–1976. [CrossRef]
15. Park, K.; Yu, B.C.; Jung, J.W.; Li, Y.; Zhou, W.; Gao, H.; Son, S.; Goodenough, J.B. Electrochemical nature of the cathode interface for a solid-state lithium-ion battery: Interface between $LiCoO_2$ and garnet-$Li_7La_3Zr_2O_{12}$. *Chem. Mater.* **2016**, *28*, 8051–8059. [CrossRef]
16. Murugan, R.; Thangadurai, V.; Weppner, W. Fast lithium ion conduction in garnet-type $Li_7La_3Zr_2O_{12}$. *Angewandte Chemie. Int. Ed.* **2007**, *46*, 7778–7781. [CrossRef]
17. Bai, Y.X.; Zhang, J.; Yang, Y.B.; Yang, R.; Yan, Y.L.; Wang, J. Enhance electrochemical performance of $LiFePO_4$ cathode material by Al-doped $Li_7La_3Zr_2O_{12}$ and carbon co-coating surface modification. *J. Alloy. Compd.* **2020**, *843*, 154915. [CrossRef]
18. Matsui, M.; Takahashi, K.; Sakamoto, K.; Hirano, A.; Takeda, Y.; Yamamoto, O.; Imanishi, N. Phase stability of a garnet-type lithium ion conductor $Li_7La_3Zr_2O_{12}$. *Dalton Trans.* **2014**, *43*, 1019–1024. [CrossRef]
19. Dermenci, K.B.; Çekiç, E.; Turan, S. Al stabilized $Li_7La_3Zr_2O_{12}$ solid electrolytes for all-solid state Li-ion batteries. *Int. J. Hydrog. Energy* **2016**, *41*, 9860–9867. [CrossRef]
20. Kotobuki, M.; Hanc, E.; Yan, B.; Molenda, J.; Lu, L. Stabilization of cubic $Li_7La_3Zr_2O_{12}$ by Al substitution in various atmospheres. *Solid State Ion.* **2020**, *350*, 115323. [CrossRef]
21. Polizos, G.; Sharma, J.; Jafta, C.J.; Muralidharan, N.; Veith, G.M.; Keum, J.K.; Kukay, A.; Sahore, R.; Wood, D.L., III. Nanostructured ligament and fiber Al–doped $Li_7La_3Zr_2O_{12}$ scaffolds to mediate cathode-electrolyte interface chemistry. *J. Power Sources* **2021**, *513*, 230551. [CrossRef]
22. Liu, X.; Gao, M.; Liu, Y.; Xiong, L.; Chen, J. Improving the room temperature ionic conductivity of Al-$Li_7La_3Zr_2O_{12}$ ceramics by Ba and Y or Ba and W co-doping. *Ceram. Int.* **2019**, *45*, 13488–13495. [CrossRef]
23. PPosch, P.; Lunghammer, S.; Berendts, S.; Ganschow, S.; Redhammer, G.J.; Wilkening, A.; Lerch, M.; Gadermaier, B.; Rettenwander, D.; Wilkening, H.M.R. Ion dynamics in Al-stabilized $Li_7La_3Zr_2O_{12}$ single crystals–Macroscopic transport and the elementary steps of ion hopping. *Energy Storage Mater.* **2020**, *24*, 220–228. [CrossRef]
24. Matsuki, Y.; Noi, K.; Suzuki, K.; Sakuda, A.; Hayashi, A.; Tatsumisago, M. Microstructure and conductivity of Al-substituted $Li_7La_3Zr_2O_{12}$ ceramics with different grain sizes. *Solid State Ion.* **2019**, *342*, 115047. [CrossRef]
25. Wolfenstine, J.; Ratchford, J.; Rangasamy, E.; Sakamoto, J.; Allen, J.L. Synthesis and high Li-ion conductivity of Ga-stabilized cubic $Li_7La_3Zr_2O_{12}$. *Mater. Chem. Phys.* **2012**, *134*, 571–575. [CrossRef]
26. Jalem, R.; Rushton, M.J.D.; Manalastas, W., Jr.; Nakayama, M.; Kasuga, T.; Kilner, J.A.; Grimes, R.W. Effects of gallium doping in garnet-type $Li_7La_3Zr_2O_{12}$ solid electrolytes. *Chem. Mater.* **2015**, *27*, 2821–2831. [CrossRef]
27. Bernuy-Lopez, C.; Manalastas, W., Jr.; Lopez del Amo, J.M.; Aguadero, A.; Aguesse, F.; Kilner, J.A. Atmosphere controlled processing of Ga-substituted garnets for high Li-ion conductivity ceramics. *Chem. Mater.* **2014**, *26*, 3610–3617. [CrossRef]
28. El Shinawi, H.; Janek, J. Stabilization of cubic lithium-stuffed garnets of the type "$Li_7La_3Zr_2O_{12}$" by addition of gallium. *J. Power Sources* **2013**, *225*, 13–19. [CrossRef]
29. Huang, X.; Su, J.; Song, Z.; Xiu, T.; Jin, J.; Badding, M.E.; Wen, Z. Synthesis of Ga-doped $Li_7La_3Zr_2O_{12}$ solid electrolyte with high Li^+ ion conductivity. *Ceram. Int.* **2021**, *47*, 2123–2130. [CrossRef]
30. Su, J.; Huang, X.; Song, Z.; Xiu, T.; Badding, M.E.; Jin, J.; Wen, Z. Overcoming the abnormal grain growth in Ga-doped $Li_7La_3Zr_2O_{12}$ to enhance the electrochemical stability against Li metal. *Ceram. Int.* **2019**, *45*, 14991–14996. [CrossRef]
31. Shen, L.; Wang, L.; Wang, Z.; Jin, C.; Peng, L.; Pan, X.; Sun, J.; Yang, R. Preparation and characterization of Ga and Sr co-doped $Li_7La_3Zr_2O_{12}$ garnet-type solid electrolyte. *Solid State Ion.* **2019**, *339*, 114992. [CrossRef]
32. Tian, Y.; Zhou, Y.; Wang, W.; Zhou, Y. Effects of Ga–Ba Co-doping on the morphology and conductivity of $Li_7La_3Zr_2O_{12}$ electrolyte synthesized by sol-gel method. *Ceram. Int.* **2021**, *48*, 963670. [CrossRef]
33. Zhang, Y.; Deng, J.; Hu, D.; Chen, F.; Shen, Q.; Zhang, L.; Dong, S. Synergistic regulation of garnet-type Ta-doped $Li_7La_3Zr_2O_{12}$ solid electrolyte by Li^+ concentration and Li^+ transport channel size. *Electrochim. Acta* **2019**, *296*, 823–829. [CrossRef]
34. Wang, Y.; Lai, W. Phase transition in lithium garnet oxide ionic conductors $Li_7La_3Zr_2O_{12}$: The role of Ta substitution and H_2O/CO_2 exposure. *J. Power Sources* **2015**, *275*, 612–620. [CrossRef]
35. Chen, X.; Wang, T.; Lu, W.; Cao, T.; Xue, M.; Li, B.; Zhang, C. Synthesis of Ta and Ca doped $Li_7La_3Zr_2O_{12}$ solid-state electrolyte via simple solution method and its application in suppressing shuttle effect of Li-S battery. *J. Alloy. Compd.* **2018**, *744*, 386–394. [CrossRef]
36. Chen, X.; Cao, T.; Xue, M.; Lv, H.; Li, B.; Zhang, C. Improved room temperature ionic conductivity of Ta and Ca doped $Li_7La_3Zr_2O_{12}$ via a modified solution method. *Solid State Ion.* **2018**, *314*, 92–97. [CrossRef]

37. Guo, H.; Su, J.; Zha, W.; Xiu, T.; Song, Z.; Badding, M.E.; Jin, J.; Wen, Z. Achieving high critical current density in Ta-doped $Li_7La_3Zr_2O_{12}$/MgO composite electrolytes. *J. Alloy. Compd.* **2021**, *856*, 157222. [CrossRef]
38. Hosokawa, H.; Takeda, A.; Inada, R.; Sakurai, Y. Tolerance for Li dendrite penetration in Ta-doped $Li_7La_3Zr_2O_{12}$ solid electrolytes sintered with $Li_{2.3}C_{0.7}B_{0.3}O_3$ additive. *Mater. Lett.* **2020**, *279*, 128481.
39. Huang, X.; Xiu, T.; Badding, M.E.; Wen, Z. Two-step sintering strategy to prepare dense Li-Garnet electrolyte ceramics with high Li^+ conductivity. *Ceram. Int.* **2018**, *44*, 5660–5667. [CrossRef]
40. He, M.; Cui, Z.; Chen, C.; Li, Y.; Guo, X. Formation of self-limited, stable and conductive interfaces between garnet electrolytes and lithium anodes for reversible lithium cycling in solid-state batteries. *J. Mater. Chem. A* **2018**, *6*, 11463–11470. [CrossRef]
41. Xue, W.; Yang, Y.; Yang, Q.; Liu, Y.; Wang, L.; Chen, C.; Cheng, R. The effect of sintering process on lithium ionic conductivity of Li6.4Al0.2La3Zr2O12 garnet produced by solid-state synthesis. *RSC Adv.* **2018**, *8*, 13083–13088. [CrossRef]
42. Huang, X.; Song, Z.; Xiu, T.; Badding, M.E.; Wen, Z. Sintering, micro-structure and Li+ conductivity of Li7−xLa3Zr2-xNbxO12/MgO (x = 0.2−0.7) Li-Garnet composite ceramics. *Ceram. Int.* **2019**, *45*, 56–63. [CrossRef]
43. Yang, T.; Li, Y.; Wu, W.; Cao, Z.; He, W.; Gao, Y.; Liu, J.; Li, G. The synergistic effect of dual substitution of Al and Sb on structure and ionic conductivity of $Li_7La_3Zr_2O_{12}$ ceramic. *Ceram. Int.* **2018**, *44*, 1538–1544. [CrossRef]
44. Xiang, X.; Chen, F.; Shen, Q.; Zhang, L.; Chen, C. Effect of the lithium ion concentration on the lithium ion conductivity of Ga-doped LLZO. *Mater. Res. Express* **2019**, *6*, 085546. [CrossRef]
45. Chen, F.; Zhang, Y.; Hu, Q.; Cao, S.; Song, S.; Lu, X.; Shen, Q. S/MWCNt/LLZO Composite Electrode with e-/S/Li^+ Conductive Network for All-Solid-State Lithium–Sulfur Batteries. *J. Solid State Chem.* **2021**, *301*, 122341. [CrossRef]
46. Goswami, N.; Indu, M.S.; Murugan, R.; Kant, R. Experimental corroboration of theory for impedance response of solid electrolytes: Doped cubic garnet LLZO. *J. Electroanal. Chem.* **2021**, *897*, 115611. [CrossRef]
47. Aravinth, K.; Ramasamy, P.; Sen, S.; Arumugam, R. Tunable photoluminescence properties of $Dy3^+$ doped LLZO phosphors for WLED and dosimetry applications. *Ceram. Int.* **2021**, *48*, 1402–1407.
48. Samui, P.; Modi, K.B.; Phapale, S.; Parida, S.C.; Mishra, R. Calorimetric investigations on lithium based ceramics. *J. Chem. Thermodyn.* **2021**, *163*, 106590. [CrossRef]
49. Wyers, G.P.; Cordfunke, E.H.P.; Ouweltjes, W. The standard molar enthalpies of formation of the lithium zirconates. *J. Chem. Thermodyn.* **1989**, *21*, 1095–1100. [CrossRef]
50. Bolech, M.; Cordfunke, E.H.P.; van Genderen, A.C.G.; van Der Laan, R.R.; Janssen, F.J.J.G.; Van Miltenburg, J.C. The heat capacity and derived thermodynamic functions of $La_2Zr_2O_7$ and $Ce_2Zr_2O_7$ from 4 to 1000 K. *J. Phys. Chem. Solids* **1997**, *58*, 433–439. [CrossRef]
51. Wang, M.; Navrotsky, A.; Venkatraman, S.; Manthiram, A. Enthalpy of Formation of LixCoO2 ($0.5 \leq x \leq 1.0$). *J. Electrochem. Soc.* **2005**, *152*, J82. [CrossRef]
52. Huntelaar, M.E.; Booij, A.S.; Cordfunke, E.H.P. The standard molar enthalpies of formation of $BaZrO_3$ (s) and $SrZrO_3$ (s). *J. Chem. Thermodyn.* **1994**, *26*, 1095–1101. [CrossRef]
53. Glushko, V.P.; Gurvich, L.V.; Bergman, G.A.; Veits, I.V.; Medvedev, V.A.; Khachkuruzov, G.A.; Yungman, V.S. *Thermodinamicheskie Svoitsva Individual'nykh Veshchestv*; Nauka: Moscow, Russia, 1978.
54. Millard, E.B. *Physical Chemistry for Colleges*; McGraw-Hill Book Company, Inc.: New York, NY, USA, 1921; ISBN-10: 1146961987.
55. Pankratz, L.B. *Thermodynamic Properties of Carbides, Nitrides, and Other Selected Substances*; Bureau of Mines: Washington, DC, USA, 1995; ISBN-10: 9995679329.
56. Lide, D.R. *CRC Handbook of Chemistry and Physics*, 86th ed.; 2005–2006; CRC Press: Boca Raton, FL, USA, 2005; pp. 4–70, ISBN 0849304865 9780849304866.
57. Samsonov, G.V. *The Oxide Handbook*; Springer: Boston, MA, USA, 1973; ISBN 978-1-4615-9597-7. [CrossRef]
58. Awaka, J.; Kijima, N.; Hayakawa, H.; Akimoto, J. Synthesis and structure analysis of tetragonal $Li_7La_3Zr_2O_{12}$ with the garnet-related type structure. *J. Solid State Chem.* **2009**, *182*, 2046–2052. [CrossRef]
59. Morachevskiy, A.G.; Sladkov, I.B.; Firsova, Y.G. *Termodinamicheskiye Raschety v Khimii i Metallurgii*; Lan': St. Petersburg, Russia, 2018; ISBN 978-5-8114-3023-9.
60. Il'ina, E.A.; Raskovalov, A.A.; Reznitskikh, O.G. Thermodynamic properties of solid electrolyte $Li_7La_3Zr_2O_{12}$. *J. Chem. Thermodyn.* **2019**, *128*, 68–73. [CrossRef]